

ROTATIONAL INSTABILITY IN THE OUTER REGION OF PROTOPLANETARY DISKS

TOMOHIRO ONO

Department of Astronomy, Graduate School of Science, Kyoto University, Sakyo-ku, Kyoto 606-8502, Japan

AND

HIDEKO NOMURA AND TAKU TAKEUCHI

Department of Earth and Planetary Sciences, Tokyo Institute of Technology, Ookayama, Meguro-ku, Tokyo 152-8551, Japan

Draft version April 1, 2014

ABSTRACT

We analytically calculate the marginally stable surface density profile for rotational instability of protoplanetary disks. The derived profile can be utilized for considering the region in a rotating disk where radial pressure gradient force is comparable to the gravitational force, such as an inner edge, steep gaps or bumps and an outer region of the disk. In this paper we especially focus on the rotational instability in the outer region of disks. We find an protoplanetary disk with a surface density profile of similarity solution becomes rotationally unstable at a certain radius, depending on its temperature profile and a mass of the central star. If the temperature is relatively low and the mass of the central star is high, disks have rotationally stable similarity profiles. Otherwise, deviation from the similarity profiles of surface density could be observable, using facilities with high sensitivity, such as ALMA.

Keywords: accretion, accretion disks - hydrodynamics - instabilities - protoplanetary disks

1. INTRODUCTION

Protoplanetary disks evolve via turbulent viscosity, and their evolution has been well represented by the model of Lynden-Bell & Pringle (1974; henceforth LBP74). In the LBP74 model, the rotation profile is assumed to be time-independent or simply Keplerian. This assumption is justified if the radial pressure gradient is much smaller than the central star gravity. The temperature in the disks is generally low enough that the radial pressure gradient can be neglected in most part of the disk. However, even in disks with low temperature, the radial pressure gradient may not be neglected in which the surface density dramatically varies in the radial direction. Such regions appear, for example, at the gap edge formed by gravity of planets, and boundary between the active and inactive regions for magneto-rotational instability. For such regions, we need to modify the LBP74 model to take into account the change in the rotation profile. Interestingly, the similarity solution of LBP74 model has an exponential cut off at the outermost region (LBP74; Hartmann et al. 1998). In the outer edge of the disk, the density decreases exponentially with a radial scale length, R_0 . Because the disk scale height, H , generally increases with the radius, the scale height become larger than the radial scale length at a certain point, resulting in violation of the assumption of negligible pressure gradient. Hence, even if there is no external force modifying the disk structure, such as photoevaporation or planets, the self-similar solution of LBP74 model itself violates self-consistency at the outer edge of the disk.

Recent development of high sensitivity (sub)millimeter interferometers makes it possible to observe surface density profiles of the outer regions of protoplanetary disks. The observations have suggested that the profiles are well fitted by similarity solution of the disks

(e.g., Hughes et al. 2008; Andrews et al. 2009, 2010; Akiyama et al. 2013), which has a sharp density profile at the outer edge. Observations using facilities with high sensitivity, such as ALMA, however, are expected to reveal the lower density area in the outer region which the radial pressure gradient force is non-negligible. Because of this, it is important that we investigate the outer region of the disks without the assumption of Keplerian disks.

When the gas pressure gradient force becomes non-negligible compared with the gravitational force in the equation of motion in the radial direction, an assumption of Keplerian rotation becomes inadequate. When we inappropriately adopt the assumption to a disk with a steep surface density profile and a large radial pressure gradient force, we often see rotational instability. Rotational instability is one of the hydrodynamical instability in axisymmetric differentially rotating disks (Chandrasekhar 1961). The Rayleigh's criterion is the discriminant for rotational stability; for an inviscid disk to be rotationally stable, the specific angular momentum (j) must monotonically increase with cylindrical distance from the axis of rotation (R) in a flow:

$$\frac{\partial j^2}{\partial R} > 0. \quad (1)$$

Otherwise, the disk becomes rotationally unstable and the gas makes radial migration with conserving specific angular momentum. In a viscid disk, viscosity limits the onset of rotational instability. Also, in the Rayleigh's criterion, the radial entropy gradient is not taken into account. We need to use the Solberg-Hoiland criterion (Endal & Sofia 1978) for a disk with a radial entropy gradient, with which the rotational instability is easier to set on in standard disks (Shakura & Sunyaev 1973). In this paper, however, we simply adopt the Rayleigh's criterion as the discriminant for rotational stability because we treat disks with low viscosity and the Rayleigh's

criterion is a more severe discriminant for rotational instability than the Solberg-Hoiland criterion.

Since the sharp edge could lead to the rotational instability, in this paper, we investigate the condition under which the disk becomes rotationally unstable. We also analytically calculate the marginally stable surface density profile for rotational instability, which indicates the profile becomes shallower than that of the similarity profile. The rotation velocity will be less than the Keplerian velocity in the region where the disk is rotationally unstable. If the deviation from the Keplerian velocity is observable, it will be an evidence that the radial pressure gradient force is sufficiently strong in the region.

We analytically examine the marginally stable disks for rotational instability in Section 2. In Section 3, we apply the result of Section 2 for protoplanetary disks. We discuss the possibility of observations of non-similarity profiles and validity of approximations used in this work in Section 4, and we summarize our conclusions in Section 5. Although many discussions here are applicable to the outer region of accretion disks in general, we focus on protoplanetary disks in this paper.

2. MARGINALLY STABLE CONDITION FOR ROTATIONAL INSTABILITY

In this section, we analytically calculate the marginally stable surface density profile for rotational instability. Then we connect the marginally stable profile to the similarity profile of viscous disks.

2.1. Rayleigh's Criterion for Protoplanetary Disks

We consider an axisymmetric rotating disk with hydrostatic equilibrium in the vertical direction. The equation for radial force balance in cylindrical coordinates is

$$\begin{aligned} \frac{j^2}{R^3} &= \frac{GM}{R^2} + \frac{1}{\rho} \frac{\partial P}{\partial R}, \\ &= \frac{GM}{R^2} + \frac{H}{\Sigma} \frac{\partial (c_s^2 \Sigma / H)}{\partial R}, \\ &= \frac{GM}{R^2} + \frac{1}{\Sigma} \frac{\partial (c_s^2 \Sigma)}{\partial R} - \frac{c_s^2}{H} \frac{\partial H}{\partial R}, \end{aligned} \quad (2)$$

where G is the gravitational constant, M the mass of the central star, P the pressure, ρ the density at mid-plane, Σ the surface density, $H \equiv c_s / \Omega_K$ the scale height, c_s the sound speed of the gas, and $\Omega_K \equiv (GM/R^3)^{1/2}$ the Keplerian angular velocity. We adopt the isothermal equation of state, $P = c_s^2 \rho$. We assume that the disk is geometrically thin $H/R \ll 1$, and that the vertical structure is isothermal, i.e., $\Sigma = \sqrt{2\pi} \rho H$.

For generalization, we define normalized non-dimensional parameters for the disk radius, r , and the surface density, σ , as follows,

$$R = R_0 r \quad \text{and} \quad \Sigma = \Sigma_0 \sigma, \quad (3)$$

where R_0 and Σ_0 are normalization constants of the disk radius and the surface density, respectively. Also, we assume that the radial temperature profile has a power-law distribution with an index, β ,

$$T = T_0 r^{-\beta}. \quad (4)$$

In this case, the radial dependences of the sound speed

and the scale height become

$$c_s = c_0 r^{-\beta/2} \quad \text{and} \quad H = H_0 r^{(3-\beta)/2}, \quad (5)$$

where T_0 , c_0 and $H_0 = c_0 / (GM/R_0^3)^{1/2}$ are the temperature, the sound speed and the scale height, respectively, at $R = R_0$.

Substituting equations (3) and (5) into equation (2), we obtain

$$\frac{j^2}{GM R_0} = r + \left(\frac{H_0}{R_0} \right)^2 r^{(2-\beta)} \left\{ \frac{\partial (\ln \sigma)}{\partial (\ln r)} - \frac{3+\beta}{2} \right\}. \quad (6)$$

Substituting equation (6) into equation (1), we obtain

$$\begin{aligned} (2-\beta) \frac{\partial (\ln \sigma)}{\partial (\ln r)} + \frac{\partial^2 (\ln \sigma)}{\partial (\ln r)^2} + \left(\frac{R_0}{H_0} \right)^2 r^{(\beta-1)} \\ - \frac{1}{2} (3+\beta)(2-\beta) > 0, \end{aligned} \quad (7)$$

where we use $r > 0$. The disk is rotationally stable when the surface density profile satisfies this condition (see also Yang & Menou 2010).

2.2. Marginally Stable Surface Density Profile for Rotational Instability

When the disk is marginally stable for rotational instability, the specific angular momentum is constant, $\partial j / \partial R = 0$. From equation (7), this condition is equivalent to

$$\begin{aligned} (2-\beta) \frac{\partial (\ln \sigma)}{\partial (\ln r)} + \frac{\partial^2 (\ln \sigma)}{\partial (\ln r)^2} + \left(\frac{R_0}{H_0} \right)^2 r^{(\beta-1)} \\ - \frac{1}{2} (3+\beta)(2-\beta) = 0. \end{aligned} \quad (8)$$

The solution of equation (8) is σ_{ms} ,

$$\begin{aligned} \sigma_{ms} = \exp \left[\frac{C_1}{(\beta-2)} r^{(\beta-2)} - \frac{1}{\beta-1} \left(\frac{R_0}{H_0} \right)^2 r^{(\beta-1)} \right. \\ \left. + \frac{3+\beta}{2} \ln r + C_2 \right], \end{aligned} \quad (9)$$

$$\frac{\partial (\ln \sigma_{ms})}{\partial (\ln r)} = C_1 r^{(\beta-2)} - \left(\frac{R_0}{H_0} \right)^2 r^{(\beta-1)} + \frac{3+\beta}{2}, \quad (10)$$

$$\begin{aligned} \frac{\partial^2 (\ln \sigma_{ms})}{\partial (\ln r)^2} = (\beta-2) C_1 r^{(\beta-2)} \\ - (\beta-1) \left(\frac{R_0}{H_0} \right)^2 r^{(\beta-1)}, \end{aligned} \quad (11)$$

where C_1, C_2 are constants of integration. Equation (9) represents the marginally stable surface density profile for rotational instability.

2.3. Rotational Instability in Viscous Disks

Here, we examine the critical radius where rotational instability occurs in the similarity solution of LBP74 model. The surface density evolution of viscous disks rotating with the Keplerian velocity is given by (e.g., Pringle 1981)

$$\frac{\partial \Sigma}{\partial t} = \frac{3}{R} \frac{\partial}{\partial R} \left[R^{1/2} \frac{\partial}{\partial R} (R^{1/2} \nu \Sigma) \right], \quad (12)$$

where t is the time and ν is the coefficient of kinematic viscosity. In the α -viscous disk model (Shakura & Sunyaev 1973), the viscosity ν is given by

$$\nu = \alpha c_s H \propto r^{(3/2-\beta)}, \quad (13)$$

where α is the standard viscous parameter and equation (5) is used. The similarity solution of equation (12) is given by Lynden-Bell & Pringle (1974) (see also Hartmann et al. 1998)

$$\Sigma = \frac{C}{3\pi\nu_1} T^{-5/(1+2\beta)} r^{(\beta-\frac{3}{2})} \exp \left[-r^{(\beta+1/2)} \right], \quad (14)$$

$$R_0 \equiv T^{2/(1+2\beta)} R_1, \quad (15)$$

where R_1 is an initial radial scale factor, C is a scaling constant and ν_1 is the coefficient of viscosity at R_1 . We note that the disk radius is normalized by R_0 , which is equal to R_1 at $t = 0$ and increases with time. While Hartmann et al. (1998) used the normalization constant R_1 , we use R_0 instead since it is more convenient for comparison with the marginally stable state discussed in Section 2.2. The non-dimensional time T is

$$T \equiv \frac{t}{T_\nu} + 1, \quad (16)$$

where the viscous scaling time, T_ν , is

$$T_\nu \equiv \frac{4}{3(1+2\beta)^2} \frac{R_1^2}{\nu_1}. \quad (17)$$

In equation (15) we set R_0 increasing with time. We set the surface density normalization constant is

$$\Sigma_0 = \frac{C}{3\pi\nu_1} T^{-5/(1+2\beta)}. \quad (18)$$

Then the non-dimensional surface density (σ_s) becomes

$$\sigma_s = r^{(\beta-\frac{3}{2})} \exp \left[-r^{(\beta+1/2)} \right], \quad (19)$$

$$\frac{\partial(\ln \sigma_s)}{\partial(\ln r)} = -(\beta + \frac{1}{2}) r^{(\beta+1/2)} + (\beta - \frac{3}{2}). \quad (20)$$

The radius at which the disk becomes rotationally unstable, r_m , is given by substituting equation (19) to equation (8)

$$\left(\frac{R_0}{H_0} \right)^2 = \frac{5}{2} \left(\beta + \frac{1}{2} \right) r_m^{3/2} + \frac{1}{2} (6 - \beta) (2 - \beta) r_m^{(1-\beta)}. \quad (21)$$

In the outer most part of the disk, $r > r_m$, the similarity profile can't be maintained because of rotational instability. Figure 1 shows the relation between r_m and H_0/R_0 given by equation (21) with $\beta = 0$ (red solid line), $\beta = 1/2$ (green dashed line) and $\beta = 3/4$ (blue dotted line). As discussed in Sect. 4.1 below, H_0/R_0 of typical protoplanetary disks ranges from 0.1 to 0.3. The critical radius r_m is about 10, 3 and 1 for $H_0/R_0 = 0.1$, 0.2 and 0.3, respectively (see Fig. 1).

In this paper, we simply assume the similarity profile connects smoothly to the marginally stable profile, i.e., $\sigma_{ms} = \sigma_s$ and $\partial\sigma_{ms}/\partial r = \partial\sigma_s/\partial r$ at $r = r_m$ (e.g. Tanigawa & Ikoma 2007). Then, from equations (9), (10), (19)-(21), the constants of integration, C_1 and C_2 ,

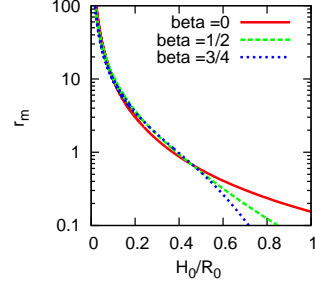


Figure 1. The relation between r_m and H_0/R_0 obtained by equation (21) for $\beta = 0$ (red solid line), $\beta = 1/2$ (green dashed line) and $\beta = 3/4$ (blue dotted line).

are obtained as

$$C_1 = \frac{3}{2} \left(\beta + \frac{1}{2} \right) r_m^{5/2} + \frac{1}{2} (1 - \beta) (6 - \beta) r_m^{(2-\beta)}, \quad (22)$$

$$C_2 = -\frac{C_1}{\beta - 2} r_m^{(\beta-2)} + \frac{\beta - 6}{2} \ln r_m + \frac{3(2\beta + 3)}{4(\beta - 1)} r_m^{(\beta+\frac{1}{2})} + \frac{(2 - \beta)(6 - \beta)}{2(\beta - 1)}. \quad (23)$$

This assumption, however, has to be examined and we will discuss more realistic evolution of the surface density profile in Sect. 4.3.

3. DEVIATION FROM THE SIMILARITY PROFILE IN THE OUTER DISKS

In this section, we investigate surface density profiles of the outer region of protoplanetary disks for two different temperature profiles. In the disks the temperature profile is controlled by irradiation from the central star and approximately proportional to $r^{-1/2}$, that is, $\beta \sim 1/2$ (e.g., Kenyon & Hartmann 1987; Chiang & Goldreich 1997; D'Alessio et al. 1998). In the outer disk where contribution of the irradiation from the central star is weak, or if the disks are irradiated by nearby massive stars, the radial temperature profile becomes roughly isothermal, that is, $\beta \sim 0$ (e.g., Robberto et al. 2002; Walsh et al. 2013). Here we simply assume a smooth connection from the similarity profile to the marginally stable profile. Furthermore, we discuss rotation velocity in the outer region of the disks where the similarity solution is not applicable.

3.1. Surface Density Profiles

3.1.1. Disks Irradiated by the Central Stars ($\beta = 1/2$)

The similarity profile of the surface density of the disks is given by equation (19)

$$\sigma_s = r^{-1} \exp(-r). \quad (24)$$

The critical radius where the profile becomes rotationally unstable, r_m , is given by equation (21)

$$\left(\frac{R_0}{H_0} \right)^2 = \frac{5}{2} r_m^{3/2} + \frac{33}{8} r_m^{1/2}. \quad (25)$$

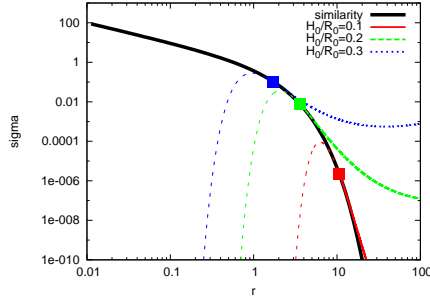


Figure 2. The surface density profile σ as a function of radial distance from the central star r in disks with $\beta = 1/2$. Black solid line shows the similarity profile. Other lines show the marginally stable profiles, which smoothly connect to the similarity profile at r_m , for $H_0/R_0 = 0.1$ (red solid line), $H_0/R_0 = 0.2$ (green long dashed line), and $H_0/R_0 = 0.3$ (blue dotted line). Each square point represents r_m .

The marginally stable surface density profile for $\beta = 1/2$ in equation (9) is

$$\sigma_{ms} = \exp \left[-\frac{2}{3}C_1 r^{-3/2} + 2 \left(\frac{R_0}{H_0} \right)^2 r^{-1/2} + \frac{7}{4} \ln r + C_2 \right]. \quad (26)$$

Smooth connection of the similarity profile to the marginally stable profile at $r = r_m$, gives the constants of integration, (equations (22) and (23))

$$C_1 = \frac{3}{2}r_m^{5/2} + \frac{11}{8}r_m^{3/2}, \quad (27)$$

$$C_2 = \frac{2}{3}C_1 r_m^{-3/2} - \frac{11}{4} \ln r_m - 6r_m - \frac{33}{4}. \quad (28)$$

Figure 2 shows the surface density profile σ as a function of radial distance from the central star r in disks with $\beta = 1/2$. Black solid line shows the similarity profile. Other lines show the marginally stable profiles, which smoothly connect to the similarity profile at r_m , for $H_0/R_0 = 0.1$ (red solid line), $H_0/R_0 = 0.2$ (green long dashed line), and $H_0/R_0 = 0.3$ (blue dotted line). Each square point represents r_m . It is apparent that for $r > r_m$ the marginally stable profile deviates from the similarity profile. It is also possible to construct marginally stable profiles for $r < r_m$, as shown by the dashed lines, but the similarity profile (black solid line) should be realized in $r < r_m$ in actual disks. For $H_0/R_0 = 0.1$, the marginally stable profile appears only at the extremely low density region (see the red line). This is because the critical radius r_m , which location is shown by the red square, is much further than the disk radius, $r = 1$, of the similarity solution, i.e., $r_m \gg 1$ (see also Fig. 1). In such disks, deviation from the similarity profile would be hardly detectable. However, for thicker disks (for larger H_0/R_0), the critical radius r_m decreases, and the marginally stable profile appears at inner part of the disk where the gas density is higher (see green long dashed and blue dotted lines). It is apparent that for $H_0/R_0 = 0.3$ the marginally stable profile (the blue dotted line) significantly deviates from the similarity profile, keeping relatively high density. In such geometrically thick disks, it is expected that the deviation from the similarity profile will be detected by future observations of high sensitivity.

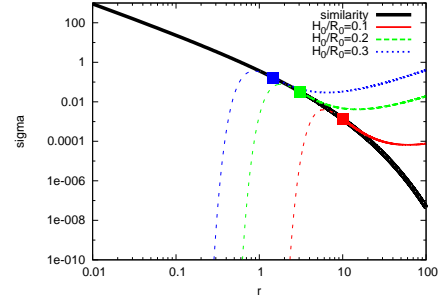


Figure 3. The same as Fig. 2, but in isothermal disks ($\beta = 0$).

3.1.2. Isothermal Disks ($\beta = 0$)

The similarity profile of the surface density of the disks is given by equation (19):

$$\sigma_s = r^{-3/2} \exp(-\sqrt{r}). \quad (29)$$

The critical radius is given by equation (21):

$$\left(\frac{R_0}{H_0} \right)^2 = \frac{5}{4}r_m^{3/2} + 6r_m. \quad (30)$$

The marginally stable surface density profile of the disks is

$$\sigma_{ms} = \exp \left[-\frac{C_1}{2}r^{-2} + \left(\frac{R_0}{H_0} \right)^2 r^{-1} + \frac{3}{2} \ln r + C_2 \right]. \quad (31)$$

The constants of integration are

$$C_1 = \frac{3}{4}r_m^{5/2} + 3r_m^2, \quad (32)$$

$$C_2 = \frac{C_1}{2}r_m^{-2} - 3 \ln r_m - \frac{9}{4}r_m - 6. \quad (33)$$

Figure 3 shows the surface density profile σ as a function of radial distance from the central star r in isothermal disks ($\beta = 0$). As with Fig. 2, black solid line shows the similarity profile and other lines show the marginally stable profiles, which smoothly connect to the similarity profile at r_m , for $H_0/R_0 = 0.1$ (red solid line), $H_0/R_0 = 0.2$ (green long dashed line), and $H_0/R_0 = 0.3$ (blue dotted line). Each square point represents r_m . Compared to the $\beta = 1/2$ case (Fig. 2), in isothermal disks the marginally stable profile outside r_m more significantly deviates from the similarity solution. Even if $H_0/R_0 = 0.1$ (red solid line), the marginally stable region appears in high surface density region. This is because the similarity profile for $\beta = 0$ (black solid line in Fig. 3) drops more slowly in the outer region than for $\beta = 1/2$ (black solid line in Fig. 2). In disks with shallower temperature profiles, the deviation from the similarity profile is more easily detectable. We note that geometrically thin approximation is broken in the region where the surface density increases (see Sect. 4.2).

3.2. Rotation Velocity Profiles

In the marginally stable region ($r \geq r_m$), the specific angular momentum is uniform ($j(r) = j(r_m)$) because $\partial j / \partial R = 0$. The rotation velocity (v_ϕ) in $r \geq r_m$ is

given by

$$v_\phi \equiv \frac{j}{R} = \sqrt{\frac{GM r_m}{R_0}} r^{-1}, \quad (34)$$

which decreases more steeply than the Keplerian profile $v_K \equiv \sqrt{GM/R_0} r^{-1/2}$, and thus it is slower than the Keplerian velocity. In reality, the specific angular momentum j would increase gradually with r (see sect. 4.3) but $(\partial j/\partial R)$ is suppressed. If $(\partial j/\partial R)$ is significantly reduced, v_ϕ should be much smaller than v_K , and deviation of rotation velocity from the Keplerian velocity profile can be observable in this region ($r > r_m$).

The deviation of rotation velocity also causes strong drag forces between dust grains and the gas. Dust grains migrate toward the central star and the drag forces make a difference between the surface density profile of the gas and dust grains. Observations indicate the difference (e.g. Panic et al. 2009) and there are some theoretical works (e.g. Takeuchi et al. 2005; Birnstiel & Andrews 2014) in order to explain the observations. These theoretical works, however, have not taken into account rotational instability and assume the similarity profiles of the disk gas, that is, they have taken into account the effect of non-Keplerian rotation of the gas for the dust evolution but not for the gas evolution (see Sect. 4.3 for details). The gas disk profile deviates from the similarity profile in non-Keplerian disks, which affects the dust disk profile. Because future observations of the outer structure of disks, by e.g. ALMA, are expected to unveil both the gas and dust disk structures, theoretical investigations on the gas and dust evolution in non-Keplerian disks is an important topic.

4. DISCUSSIONS

4.1. Possibility of Observational Detection of Non-Similarity Profiles

In this section, we discuss the possibility of observational detection of non-similarity profiles in protoplanetary disks, which depends on the value of H_0/R_0 . In typical T Tauri disks, the scale height is roughly estimated as

$$\frac{H}{R} \approx 0.1 \left(\frac{T}{28K} \right)^{1/2} \left(\frac{M_*}{M_\odot} \right)^{-1/2} \left(\frac{R}{100AU} \right)^{1/4}, \quad (35)$$

where we assume $T = 280K$ at $R = 1AU$ and adopt $\beta = 1/2$, considering that the temperature profile is controlled by the central star. In the outer regions where the temperature is as low as that of the surrounding molecular clouds ($\sim 10 - 30K$, depending on low or high mass star forming regions), the temperature profile approaches isothermal ($\beta = 0$, see below). Observationally, R_0 ranges from $\sim 15AU$ to $200AU$ (Andrews et al. 2009, 2010), and then $H_0/R_0 \sim 0.1 - 0.18$ from equation (35) if we adopt $M_* = 0.5M_\odot$. In this case, $r_m = R_m/R_0$ is roughly 3-10 (see Fig. 1). For disks with a relatively less massive central star and relatively high temperature, H_0/R_0 would be close to 0.2. For such disks, deviation of surface density from the similarity profile is so large near R_m that the deviation will be detected by future observations. If H_0/R_0 is as low as 0.1, it will be hard to observe the deviation (see Fig. 2). We note that Andrews & Williams (2007) reported some

deviation from the similarity profiles in their observations of surface density profiles of protoplanetary disks. In typical Herbig Ae disks, the temperature is higher ($T \approx 100K$ at $R = 10AU$; e.g., Dullemond & Dominik 2004) but the stellar mass is larger ($M_* \approx 2M_\odot$). Therefore, H_0/R_0 becomes smaller and the deviation seems more difficult to observe.

For disks irradiated by nearby massive stars in young clusters, the external irradiation makes $\beta \simeq 0$ in the outer regions as in the case of protoplanetary disks in the Trapezium Cluster in the Orion Nebula (e.g., Robberto et al. 2002; Walsh et al. 2013). In this case, the scale height is roughly estimated as

$$\frac{H}{R} \approx 0.2 \left(\frac{T}{60K} \right)^{1/2} \left(\frac{M_*}{0.5M_\odot} \right)^{-1/2} \left(\frac{R}{100AU} \right)^{1/2} \quad (36)$$

where we assume $T = 60K$ in the outer region and adopt $\beta = 0$. H_0/R_0 approaches about 0.3 if the mass of the central star is as low as $\sim 0.2M_\odot$ (e.g., Hillenbrand et al. 1998). In this case, $r_m = R_m/R_0$ is roughly 1 (see Fig. 1), and the deviation from the similarity profile is possibly observable (see Fig. 3). In disks near a massive star, however, the gas in the outer region escapes due to photoevaporation, which should be taken into accounts, (e.g., Johnstone et al. 1998; Richling & Yorke 2000). On the other hand, our result also suggests that radial pressure gradient force may affect evolution process due to photoevaporation by surrounding high mass stars (see Sect. 4.3).

To summarize, it is expected that deep observations in near future can detect deviation from the similarity profile of surface density in the outer regions of the disks whose central stars are less massive and temperature is relatively high. In the disks heated by irradiation from a nearby massive star in young star clusters, the deviation will be more easily observable, but we should take into account the effect of photoevaporation on the surface density profile in the outer disks. Observations by facilities with high sensitivity, such as ALMA, will reveal the surface density profiles of the outer regions of protoplanetary disks, which tell us physical properties of disks with sharp surface density profiles.

4.2. Break of Geometrically Thin Approximation in The Outer Region

In this paper, we assume that disks are geometrically thin. The assumption, however, breaks in the outer region of the disks. From equations (3) and (5), the scale height is given by

$$\frac{H}{R} = \frac{H_0}{R_0} r^{(1-\beta)/2}. \quad (37)$$

Figure 4 shows the scale height, H_m , at $R_m \equiv R_0 r_m$ as a function of H_0/R_0 , obtained by equations (3), (5) and (21) for $\beta = 0$ (red solid line), $\beta = 1/2$ (green dashed line) and $\beta = 3/4$ (blue dotted line). Because $H_m/R_m \sim 0.4$ at most, the figure indicates that geometrically thin approximation is appropriate around R_m . Beyond r_m , H/R exceeds unity around the minimum point of the marginally stable surface density profile in Figs. 2 and 3 (for $\beta = 1/2$, $r \sim 10^4$, 625 and 100, and for $\beta = 0$, $r \sim 100$, 25 and 10 for $H_0/R_0 = 0.1$, 0.2 and 0.3, respectively) and the geometrically thin approximation

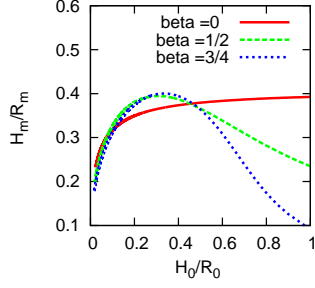


Figure 4. The relation between H_m/R_m and H_0/R_0 obtained by equations (3), (5) and (21) for $\beta = 0$ (red solid line), $\beta = 1/2$ (green dashed line) and $\beta = 3/4$ (blue dotted line).

is invalid beyond the radius. If the gas of the surrounding envelope continues to infall to the disk, the density profile in the outer edge may be more shallower than the self-similar profile. In order to consider this situation, let the density profile be a simple power-law in the whole disk. In this case, R_m would be larger compared to the disk of similarity profiles, resulting in break-down of the geometrically thin approximation around R_m (see equations (8) and (37)). The steep drop of the density at the exponential tail is essential to cause rotational instability.

4.3. Evolution of Surface Density Profile in the Outer Region

In the previous sections, we simply assume that the surface density profiles connect smoothly from the similarity profile to the marginally stable profile at r_m . In reality, the surface density profile evolves so that it avoids to be rotationally unstable. In this subsection we discuss time evolution of the surface density profile. Here, we use only three approximations that disks are axisymmetric and geometrically thin and self-gravitation of disks is negligible. Now, the equation of continuity is

$$R \frac{\partial \Sigma}{\partial t} + \frac{\partial}{\partial R} (R \Sigma v_R) = 0, \quad (38)$$

the equation of motion in the radial direction is

$$\frac{\partial v_R}{\partial t} + v_R \frac{\partial v_R}{\partial R} - \frac{j^2}{R^3} = -\frac{1}{\rho} \frac{\partial P}{\partial R} - \frac{GM}{R^2}, \quad (39)$$

and the equation of angular momentum transfer is

$$2\pi R \Sigma \frac{\partial j}{\partial t} - \dot{M} \frac{\partial j}{\partial R} = \frac{\partial W}{\partial R}, \quad (40)$$

where v_R is the velocity of the gas in the radial direction, \dot{M} is the inward mass flux, W is the viscous torque caused by turbulent motion. \dot{M} is defined as

$$\dot{M} \equiv -2\pi R \Sigma v_R. \quad (41)$$

W is defined as

$$W \equiv 2\pi R^2 T_{R\varphi} = 2\pi R^3 \nu \frac{\partial \Omega}{\partial R}, \quad (42)$$

where φ is the azimuthal component in the cylindrical coordinate system, $T_{R\varphi}$ is the $R\varphi$ component of the viscous stress tensor. We assume the other components of

the viscous stress tensor are negligible. Using equations (41) and (42), equations (38)-(40) are

$$\frac{\partial \Sigma}{\partial t} = \frac{1}{2\pi R} \frac{\partial \dot{M}}{\partial R}, \quad (43)$$

$$\frac{\partial \dot{M}}{\partial t} = -2\pi R \Sigma \left(\frac{j^2}{R^3} - \frac{GM}{R^2} - \frac{1}{\rho} \frac{\partial P}{\partial R} \right) - \frac{\dot{M}^2}{2\pi R^2 \Sigma} \left(1 + \frac{\partial \ln \Sigma}{\partial \ln R} - 2 \frac{\partial \ln \dot{M}}{\partial \ln R} \right), \quad (44)$$

$$\frac{\partial j}{\partial t} = \frac{1}{2\pi R \Sigma} \left(\dot{M} \frac{\partial j}{\partial R} + \frac{\partial W}{\partial R} \right). \quad (45)$$

Equation (43)-(45) are differential equations of $\Sigma(R, t)$, $\dot{M}(R, t)$ and $j(R, t)$.

In the previous sections, we ignore the terms which contain second-order of \dot{M} and the terms of $(\partial \dot{M}/\partial t)$ and $(\partial j/\partial t)$. In general, we can't ignore these terms when $\partial j/\partial R$ approaches 0. Here, in order to comprehend qualitatively how the surface density profile evolves when $\partial j/\partial R$ approaches 0, we retain only the term which contains second-order of \dot{M} , ignoring the terms $(\partial \dot{M}/\partial t)$ and $(\partial j/\partial t)$. Then equations (43)-(45) are rewritten as

$$\frac{\partial \Sigma}{\partial t} = \frac{1}{R} \frac{\partial}{\partial R} \left[\frac{1}{\left(\frac{\partial j}{\partial R} \right)} \frac{\partial}{\partial R} \left\{ \nu j \Sigma \left(2 - \frac{\partial \ln j}{\partial \ln R} \right) \right\} \right], \quad (46)$$

$$j^2 = GMR + \frac{R^3}{\rho} \frac{\partial P}{\partial R} - \frac{1}{\Sigma^2 \left(\frac{\partial j}{\partial R} \right)^2} \left[\frac{\partial}{\partial R} \left\{ \nu j \Sigma \left(2 - \frac{\partial \ln j}{\partial \ln R} \right) \right\} \right]^2 \left(1 + \frac{\partial \ln \Sigma}{\partial \ln R} - 2 \frac{\partial \ln \dot{M}}{\partial \ln R} \right), \quad (47)$$

$$\dot{M} = \frac{2\pi}{\left(\frac{\partial j}{\partial R} \right)} \frac{\partial}{\partial R} \left\{ \nu j \Sigma \left(2 - \frac{\partial \ln j}{\partial \ln R} \right) \right\}. \quad (48)$$

Equation (46) is the evolution of the surface density of a geometrically thin viscous disks (similar to equation (12), but without an assumption of the Keplerian rotation) and equation (47) is the equation for radial force balance (similar to equation (2)). Equations (46) and (48) indicate that when $(\partial j/\partial R)$ approaches 0 around $R \sim R_m$, the surface density diffuses fast and \dot{M} becomes large, and then the third term on right side of equation (47) becomes non-negligible. However, since the diffusion velocity should be subsonic, the accretion rate is limited to $|\dot{M}| = 2\pi R \Sigma c_s$. In this case, $(\partial j/\partial R)$ is roughly estimated from equation (48) as

$$\begin{aligned} \frac{\partial j}{\partial R} &= \frac{2\pi}{\dot{M}} \frac{\partial}{\partial R} \left\{ \nu j \Sigma \left(2 - \frac{\partial \ln j}{\partial \ln R} \right) \right\} \\ &\sim \frac{2\pi}{2\pi R \Sigma c_s} \frac{1}{R} (2\alpha c_s H j \Sigma) \\ &\sim \alpha c_s \Omega / \Omega_K, \end{aligned} \quad (49)$$

where we adopt $\nu = \alpha c_s H$, $H = c_s / \Omega_K$ and $j = \Omega R^2$. Thus, around $R \sim R_m$, $(\partial j/\partial R)$ is much smaller than

that of the disk rotating with the Keplerian velocity, $\partial j/\partial R \sim v_K$, since $c_s < v_K$ and $\Omega < \Omega_K$. Therefore, the surface density profile around $R \sim R_m$ will be close to the marginally stable profile, σ_{ms} , obtained in Sect.3.1. But it is not exactly the same as σ_{ms} since $\partial j/\partial R \neq 0$. In order to obtain the actual surface density profile, we need to solve equations (43)-(45) in future work.

5. SUMMARY

In this paper, the surface density profile of the outer region of protoplanetary disks is discussed. We find that the similarity solution is not realized in the outer region due to rotational instability. The surface density at the outer region drops with r more slowly than the similarity profile, and is expected to approach the marginally stable profile. The deviation from the similarity profile becomes more significant for larger H_0/R_0 and for shallower radial temperature profiles. In order to detect the deviation from the similarity profile, we propose to observe the disks whose central stars are less massive and whose temperature is relatively high. In this paper, we calculate the surface density profiles simply assuming the smooth connection of the marginally stable profile to the similarity profile at a critical radius r_m in order to study qualitative behavior of the surface density profile. For quantitative comparison to the disk observations, we need to calculate time evolution of the surface density and the rotation velocity simultaneously, as discussed in section 4.3. Application to other kinds of accretion disks also remains as future work.

We thank Hidekazu Tanaka, Takayuki Muto and Shin Mineshige for their useful comments, which greatly improved the discussions in the manuscript. We are also grateful to the referee who helped improve the quality of the manuscript. This work was partly supported by Grant-in-Aids for Scientific Research, 23103005 and

25400229.

REFERENCES

- Akiyama, E., Momose, M., Kitamura, Y., Tsukagoshi, T., Shimada, S., Koyamatsu, S., Hayashi, M., 2013, PASJ...65..123
 Andrews, S. M. and Williams, J. P., 2007, ApJ...659..705
 Andrews, S. M., Wilner, D. J., Hughes, A. M., Qi, C., and Dullemond, C. P., 2009, ApJ...700.1502
 Andrews, S. M., Wilner, D. J., Hughes, A. M., Qi, C. and Dullemond, C. P., 2010, ApJ...723.1241
 Birnstiel, T. and Andrews, S. M., 2014, ApJ...780..153
 Chandrasekhar, S., "Hydrodynamic and hydromagnetic stability", International Series of Monographs on Physics, Oxford: Clarendon, 1961
 Chiang, E. I. and Goldreich, P., 1997, ApJ...490..368
 D'Alessio, P., Canto, J., Calvet, N. and Lizano, S., 1998, ApJ...500..411
 Dullemond, C. P. and Dominik, C., 2004, A&A, 417, 159
 Endal, A. S. and Sofia, S., 1978, ApJ...220..279
 Hartmann, L., Calvet, N., Gullbring, E. and D'Alessio, P., 1998, ApJ...495..385
 Hillenbrand, L. A. Strom, S. E., Calvet, N. et al. 1998, AJ, 116, 1816
 Hughes, A. M., Wilner, D. J., Qi, C. and Hogerheijde, M. R. , 2008, ApJ...678.1119
 Johnstone, D., Hollenbach, D. and Bally, J., 1998, ApJ...499..758
 Kenyon, S. J. and Hartmann, L., 1987, ApJ...323..714
 Lynden-Bell, D. and Pringle, J. E., 1974, MNRAS.168..603
 Panić, O. and Hogerheijde, M. R. and Wilner, D. and Qi, C., 2009, A&A...501..269
 Pringle, J. E., 1981, ARA&A..19..137
 Richling, S. and Yorke, H. W., 2000, ApJ...539..258
 Robberto, M., Beckwith, S. V. W. and Panagia, N., 2002, ApJ...578..897
 Shakura, N. I. and Sunyaev, R. A., 1973, A&A....24..337
 Takeuchi, T. and Clarke, C. J. and Lin, D. N. C., 2005, ApJ...627..286
 Tanigawa, T. and Ikoma, M., 2007, ApJ...667..557
 Walsh, C., Millar, T. J. and Nomura, H., 2013, ApJ...766L..23
 Yang, C.-C. and Menou, K., 2010, MNRAS.402.2436